Colloids and Surfaces A: Physicochemical and Engineering Aspects 664 (2023) 131125

Contents lists available at ScienceDirect

Colloids and Surfaces A: Physicochemical and Engineering Aspects

journal homepage: www.elsevier.com/locate/colsurfa

Stability of supported hybrid lipid bilayers on chemically and topographically-modified surfaces

Laure Bar [a], Martín Eduardo Villanueva [a], Claudio Martín [a], Andrea Valencia Ramirez [b,c], Jonathan Goole [d], Frank Uwe Renner [b,c], Patricia Losada-Pérez [a,*]

[a] Experimental Soft Matter and Thermal Physics (EST) group, Department of Physics, Université libre de Bruxelles, Boulevard du Triomphe CP223, 1050 Brussels, Belgium
[b] Institute for Materials Research, Hasselt University, Wetenschapspark 1, 3590 Diepenbeek, Belgium
[c] IMEC vzw, Division IMOMEC, Wetenschapspark 1, 3590 Diepenbeek, Belgium
[d] Laboratory of Pharmaceutics and Biopharmaceutics, Université libre de Bruxelles, Campus de la Plaine, CP 207, Boulevard du Triomphe, Brussels 1050, Belgium

HIGHLIGHTS

- Polar component of the substrate surface energy modulates effective formation of supported lipid bilayers.
- Gel phase or gel domains preclude global lipid vesicle rupture.
- Hybrid lipid bilayers exhibit decoupled nanomechanical responses.
- Spatially controlled hybrid and pure lipid bilayers coexist on micropatterned Au surfaces.

GRAPHICAL ABSTRACT

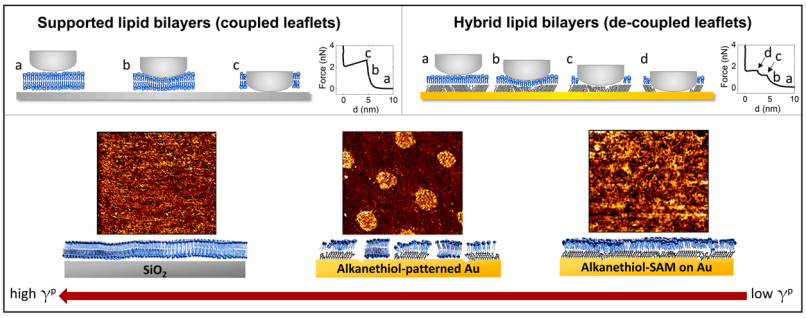

ARTICLE INFO

Keywords:
Hybrid lipid bilayers
Atomic force microscopy
Microcontact printing
Self-assembled monolayers
Force spectroscopy
Quartz crystal microbalance with dissipation
Lipid membranes

ABSTRACT

Hybrid lipid bilayers are a particular case of supported lipid bilayers with the two monolayer leaflets composed by different types of molecules. These nanostructures can be produced in a well-controlled array fashion and are suitable for the study of biomembrane-related phenomena via electrochemical or plasmonic sensing. Understanding how the underlying solid surface affects the supported membrane formation and organization is necessary for the potential use of these hybrid platforms in applications for which surfaces are not flat and topographically complex. Here we assess the role of lipid phase, substrate surface energy and topography on the formation and stability of hybrid supported membranes from vesicle precursors using complementary surface-sensitive techniques, namely quartz crystal microbalance with dissipation and atomic force microscopy. The stability of hybrid bilayers against thermal and osmotic changes is evaluated and compared to standard supported lipid bilayers formed onto hydrophilic SiO_2. Force spectroscopy measurements reveal an overall weaker lateral organization of hybrid membranes as a result of the underlying self-assembled monolayer being not optimally organized. Hybrid bilayers display a decoupled behavior between the two leaflets when vertically compressed at constant speed. On microcontact printed Au surfaces, hybrid bilayers were formed over printed

* Corresponding author.
E-mail address: patricia.maria.losada.perez@ulb.be (P. Losada-Pérez).

https://doi.org/10.1016/j.colsurfa.2023.131125
Received 22 November 2022; Received in revised form 20 January 2023; Accepted 8 February 2023
Available online 10 February 2023

patches, while surprisingly, supported lipid bilayers were observed on non-patterned Au regions suggesting a non-trivial self-assembled monolayer reorganization when in aqueous environment.

1. Introduction

Solid-supported lipid membranes are useful platforms at the solid-liquid interface with a broad range of applications, from cell membranes mimics, biosensing platforms, drug screening systems, to surface modification of medical implants [1–3]. The strategies to form supported lipid membranes are numerous, and result in different types of lipid assemblies. The most used methodologies are Langmuir–Blodgett/Schäfer, spin-coating, and vesicle fusion, which can lead to supported lipid monolayers, bilayers, hybrid bilayers, multilayers, or intact vesicles depending on the controlling parameters used for each method [4–6]. Spin-coating and Langmuir–Blodgett/Schäfer require dedicated instruments and typically lead to homogeneous lipid multilayers and monolayers/bilayers, respectively. Vesicle fusion and rupture is simpler, yet depends more on vesicle-surface interactions, which, in turn, offer the possibility of forming different supported lipid-based assemblies. There are two main types of supported lipid bilayer films (SLBs) that can be formed depending on the adhesive and electrostatic properties of the surface. For instance, very hydrophilic surfaces such as mica, SiO_2 or glass induce rupture of vesicles yielding noncovalently adsorbed SLBs with a very thin film of water in between the solid surface and the bilayer. The mechanism of formation and resulting stability of SLBs have been the subject of intensive research and it is a rather well-understood topic [6–10].

Supported lipid membranes onto hydrophobic surfaces are by far less studied and restricted to vesicle deposition onto silanized surfaces, graphene and more often onto alkanethiol self-assembled monolayers (SAMs) [11–13]. Hybrid lipid bilayers are typically formed onto SAM-modified Au surfaces, resulting in a thiolated-alkyl chain covalently bound to the surface as lower leaflet, and a lipid monolayer as upper leaflet. The lower leaflet is supposed to confer the hybrid bilayer superior stability against changes in buffer composition and pH [13].

On very hydrophobic SAM-modified surfaces, the exposure of the hydrophobic monolayer to the aqueous environment is thermodynamically unfavorable and leads to vesicle rupture to cover the SAM with a lipid monolayer for energy minimization. The rupture mechanism is rather complex and proceeds by vesicle destabilization followed by strong interactions between the surface and the hydrophobic core of the lipid bilayers. A mechanistic picture of the vesicle destabilization and rupture process was first provided by Kalb et al. [14], who monitored adsorption of small unilamellar lipid vesicles using total internal reflection microscopy combined with fluorescence recovery after photobleaching. The proposed mechanism was vesicle hemifusion induced by a defect in the vesicle outer leaflet to enable contact between the vesicle's inner leaflet and the SAM. In order to initiate hemifusion, an energy barrier for membrane reorganization needs to be surmounted. Hemifusion occurs by spreading of outer-layer lipids to the hydrophobic surface leading to stress between the outer and inner leaflet and the formation of a pore near the contact site with the SAM [15–18]. This mechanistic picture was supported by using several methods such as neutron reflectometry [19], surface plasmon resonance [17,20], ellipsometry [21], quartz crystal microbalance with dissipation (QCM-D) [22–24] and electrochemical measurements [15,25–27]. These methods provide indirect evidence of the formation of a hybrid bilayer and average out over a large surface area.

Unlike for homogeneous SLBs formed onto very hydrophilic surfaces, the influence of parameters involving specific properties of the lipid vesicles and the SAM layer on the kinetics of the rupture process and the resulting hybrid bilayer stability remains poorly explored. Studies are restricted to varying vesicle concentration and alkanethiol chain length [13,16,23]. The kinetics of hybrid bilayer formation depends strongly on the vesicle concentration, being diffusion-limited at high concentrations, while the rate-limiting step at low concentrations is the lipid surface reorganization [16]. The successful formation of a hybrid bilayer depends on the quality of the SAM layer. Even for very hydrophobic surfaces with very low surface free energy, the presence of defects might arrest hemifusion and inhibit destabilization [13]. The packing density of the SAM depends on the alkyl chain length, as well as on the surface roughness and topography of the underlying solid surface [28]. Understanding how the underlying solid surface affects the supported lipid membrane formation and organization has been seldomly explored and it is necessary for the potential use of these platforms in real applications for which surfaces can be rough and topographically complex. Examples of potential application of hybrid lipid membranes span from fundamental physico-chemical studies involving membrane curvature [29] to potential applications such as the nano-assemblies mimicking photosynthesis [30], enzyme biorecognition platforms [31] and array chips for targeted biomolecular or cell immobilization [32].

In this paper we aim at providing insights on how the interplay between the properties of the solid support (surface energy, roughness, topography) and the lipid vesicles (bilayer phase) drives the formation and stability of homogeneous and hybrid lipid bilayers, or of supported vesicle layers (SVLs). Specifically, we use surfaces with different degrees of the polar contribution to the surface energy, i.e., very hydrophilic such as SiO_2 and very hydrophobic such as alkanethiol SAM-modified Au. Topographically complex surfaces consist of Au surfaces with localized, micrometer-sized SAM-modified regions by means of microcontact printing. The phase of lipid bilayers is controlled by using one-component vesicles displaying one phase (gel or liquid disordered) and macroscopic lipid phase separation. We combine robust surface-sensitive techniques, namely QCM-D with atomic force microscopy (AFM) and force spectroscopy (AFM-FS) measurements to assess the quality and the global and local stability of the formed supported lipid membranes. QCM-D is a label-free method that can sense in real-time very small changes in mass per unit area, thickness and viscoelastic properties of films when adsorbed on a solid surface. QCM-D is very useful to assess the kinetics and the fate of lipid vesicles upon adsorption to a solid surface since it can distinguish whether vesicles (globally) adsorb and either remain intact or break into SLBs. AFM in turn, provides information related to local topography and, with FS, nanomechanical behavior of the formed supported membrane films. The combination of these techniques is thus very appropriate to obtain a complete picture (both global and local) of the supported lipid membranes formed onto solid surfaces [10].

2. Materials and methods

2.1. Materials

1,2-dipalmitoyl-sn-glycero-3-phosphocholine (DPPC – powder form) and a solution of 1,2-dioleoyl-sn-glycero-3-phosphocholine (DOPC – dissolved in chloroform) were purchased from Avanti Polar Lipids (Alabaster, AL, USA). HEPES powder $\geq$ 99.5% (Sigma-Aldrich, Overijse, Belgium), NaCl powder $\geq$ 99% (Sigma-Aldrich, Overijse, Belgium), and NaOH powder (VWR chemicals, Leuven Belgium) were used for the buffer solution. Diiodomethane 99% (used for the contact angle measurements), and 1-hexadecanethiol (used to form SAMs were purchased from Sigma-Aldrich (Overijse, Belgium). The masses of lipids were determined gravimetrically using an analytical balance (AG245, Metter-Toledo, Switzerland) with a precision of $\pm$ 0.1 mg. The HEPES buffer (pH 7.4) used for the hydration of the dried lipid films was prepared by dissolving 10 mM HEPES and 150 mM NaCl in Milli-Q water (18.2 MΩ).

The pH was then adjusted to 7.4 with a 1 M NaOH solution (previously prepared with NaOH powder and Milli-Q water), and checked with a FiveEasy Mettler Toledo pHmeter from Mettler Toledo, Zaventem, Belgium. The buffer was then filtered with 0.2 μm-pore size polyethersulfone syringe filters (VWR chemicals, Leuven Belgium) and stored at 4 °C until being used.

2.2. Lipid vesicle preparation

Three different types of lipid vesicles dispersions were used, namely pure DOPC, pure DPPC and an equimolar mixture of DOPC and DPPC lipids. These dispersions were prepared as follows. First, dried lipid films were formed by dissolving the lipids or lipid mixtures in chloroform and drying under a gentle stream of N_2. To avoid any residues of solvent, the lipid films were kept under low pressure overnight. The films were then hydrated with fresh filtered HEPES buffer to 2 mg/ml under continuous stirring for 45 min, in a temperature-controlled water bath at temperatures well above the melting of the specific lipids used. Unilamellar vesicles were formed by extrusion through polycarbonate filters with pore size 100 nm for 25 passes. The extruded dispersions were then diluted in HEPES buffer for obtaining a working concentration of 0.1 mg/ml for QCM-D and AFM experiments.

2.3. Surface preparation

Solid surfaces with different degrees of polar component in their surface energy were used, namely bare SiO_2, bare UV-ozoned Au, and Au chemically modified with a homogeneous alkanethiol SAM or with a micropatterned alkanethiol SAM. For bare surfaces, AT-cut quartz crystals with SiO_2 or Au (polycrystalline) coating (diameter 14 mm, thickness 0.3 mm, quoted surface roughness < 2 nm, and resonant frequency 4.95 MHz) were used as solid surfaces and purchased from Quartz Pro AB (Jarfalla, Sweden). For imaging supported lipid layers using AFM, the above mentioned SiO_2-coated quartz flat crystals as well as single crystal SiO_2 surfaces with (100) orientation and roughness (RMS) $r = 0.13 \pm 0.04$ nm were used. The latter were purchased from Prime Wafers (Bergschenhoek, The Netherlands). Concerning the Au surfaces, the above-mentioned Au-coated quartz flat crystals as well as ultraflat Au surfaces with roughness (RMS) $R_q = 0.20 \pm 0.01$ nm were used for AFM measurements. The latter were purchased from Platypus Technologies (Madison, USA).

SiO_2-coated quartz sensors were cleaned by immersion for 2 h in a solution of 2% sodium dodecyl sulfate (SDS) in milli-Q water, subsequently rinsed in milli-Q water and dried with N_2. The Au-coated quartz sensors were cleaned by immersion for 5 min in a 5:1:1 mixture of milli-Q water, ammonia and hydrogen peroxide heated at 75 °C, subsequently rinsed in milli-Q water and dried with N_2. Shortly prior to the beginning of the QCM-D measurements, Au sensors were exposed to UV-light for 15 min using a UV-ozone cleaner (Bioforce Nanosciences, Wetzlar, Germany).

Homogeneous SAMs of 1-hexadecanethiol were formed on Au surfaces by overnight immersion in a 1 mM solution of 1-hexadecanethiol in absolute ethanol and kept in the dark. These surfaces were rinsed with ethanol and gently dried by N_2.

For preparing Au surfaces modified with a spatially-controlled alkanethiol SAM, microcontact printing was used. It consists of applying a micropatterned-stamp previously inked with the thiol solution to a substrate, in order to transfer the SAM patterns to the surface. In our case, polydimethylsiloxane (PDMS) stamps were fabricated by traditional photolithography techniques [33]. These stamps consist of an array of micrometer-sized circles separated by micrometer-sized distances. Prior to exposure to the alkanethiol solution, the stamps were rinsed with pure ethanol and dried under N_2 gas. Afterwards, the stamps were exposed to a droplet of 1 mM alkanethiol solution for ~ 30 s and dried gently under N_2 gas. The thiol-containing stamp was placed onto a Au surface for ~ 30 s and immediately peeled off.

2.4. Dynamic light scattering measurements

Vesicle diameters and polydispersities were determined by means of dynamic light scattering (DLS) (Malvern Zetasizer Nano ZS, Malvern, UK). Solutions of extruded vesicles diluted at 0.05 mg/ml in Hepes buffer were used. The mean diameters of vesicles consisting of pure DPPC, DPPC:DOPC mixture, and pure DOPC were 108 ± 2 nm, 114 ± 2 nm, and 114 ± 1 nm, respectively. The polydispersities were 0.09 ± 0.01, 0.09 ± 0.02, and 0.11 ± 0.01 respectively, suggesting that vesicle dispersions are rather homogeneous in size.

2.5. Density measurements

Density measurements were performed on a DSA 5000 M (Anton Paar, Graz, Austria) vibrating tube density meter from 15° to 45°C with a temperature step of 0.08 °C. The accuracies for the density and the temperature were of 0.000007 g/cm^3 and 0.01 °C, respectively. Prior to each experiment, the density meter was cleaned several times with ethanol, dried, and calibrated by measuring the densities of air and water. The pure buffer and non-extruded lipid vesicle dispersions (5 mg/ml concentration in buffer) were degassed prior to injection into the instrument to avoid the formation of air bubbles inside the tube during the heating processes. For degassing the lipid dispersions, the samples were placed into a desiccator connected to a vacuum pump. For small volumes (3 ml), one minute was enough to extract the entrapped air inside the solutions. As it will be seen in Section 3.1 of the Results and Discussion, density measurements provide temperature-dependent molecular volumes of the lipid vesicle dispersions in bulk, and, consequently, the phase behavior of the studied systems.

2.6. Contact angle measurements

Contact angle measurements were carried out using an Attension ThetaLite (Biolin Scientific, Gothenburg, Sweden) based on the sessile drop method. A small drop (3 μl) of either milli-Q water (polar liquid) or diiodomethane (apolar liquid) was deposited onto the different surfaces, and the shape of the formed drop was evaluated. The contact angle of a 3 μl droplet of ultrapure water was measured for 10 s using a recording speed of 20 frames/s at room temperature. The results of the surface energy γ_{sv} of the different surfaces under study from contact angle measurements are provided in Section 3.1 of the Results and Discussion.

2.7. Quartz crystal microbalance with dissipation monitoring

QCM-D measurements were carried out in a Qsense E4 instrument (Biolin Scientific, Gothenburg, Sweden), which enables simultaneous monitoring of frequency and dissipation changes, $\Delta f/n$ and ΔD, with n the overtone number. Real-time changes in $\Delta f/n$ and ΔD were monitored at five different overtones (from 3rd to 11th). The concentration of vesicles used in the QCM-D experiments was 0.1 mg/ml and they were injected over the solid surfaces in the QCM-D flow cells at 50 μl/min for 10 min. The QCM-D experiments carried out in this work comprise two stages: (i) Lipid vesicle adsorption onto surfaces with different degrees of surface energy at constant temperature $T = 25 \pm 0.02$ °C and signal stabilization for 5 h, (ii) heating and cooling cycles from 16 °C to 50 °C at 0.4 °C/min to assess the phase transition behavior of the formed supported lipid membrane layers (either SVL or SLB).

2.8. Atomic force microscopy

AFM measurements were performed using a JPK Nanowizard 4 BIO-AFM from Bruker (Nano GmbH, Berlin, Germany). Images of the bare solid surfaces were performed using AC-mode (tapping) in air using PPP-NCL-W probes (Nanosensors, Neuchatel, Switzerland) with a cantilever length of ~ 225 μm, resonance frequency of ~ 150 kHz, and spring constant of ~ 48 N/m. AC-mode provides high-resolution images of the

solid surfaces (topography and average roughness). AFM measurements made on lipid films were performed in buffer by either using the flat SiO_2 and Au substrates, or the SiO_2 and Au coated quartz crystals. In the first case, the bare or chemically-modified surfaces were directly placed inside the AFM fluid cell, and were incubated in the lipid solutions for 30 min. For each experiment, the surfaces were rinsed several times with pure buffer while keeping the substrates submerged into the solution. To verify the observed results obtained with the ex-situ method, the quartz crystals were also analyzed after a lipid adsorption and rinsing performed inside the QCM-D. The surface transfer between the QCM-D chambers and the AFM fluid cell was carefully carried out to avoid the dewetting. The results obtained for both type of surfaces (wafers vs quartz crystals) were always consistent, except for the case of DOPC: DPPC layers adsorbed onto SiO_2, which will be developed in the AFM results section 3.3.1.

AFM measurements including SVLs or SLBs on the different surfaces were performed in liquid using Quantitative imaging (QI) mode and MLCT-E probes (Bruker, Ca, USA) with quoted cantilever length of L ~ 140 μm, resonance frequency of ~38 kHz, and nominal tip radius of 20 nm. The AFM cantilevers were calibrated in buffer against a clean glass slide according to the thermal noise method [34]. The determined sensitivities and spring constants were always in the ranges of 14 − 19 nm/V and 0.18 − 0.2 N/m, respectively. Measurements were carried out at T = 25 °C ± 1 °C. QI images were taken at different scan sizes using a sampling of 256 × 256 pixels and setpoint force of 300 pN. In order to assess the nanomechanical properties of the supported membranes, force maps over square grids with 16 × 16 points were performed with a force spectroscopy curve recorded per point. For each sample, several square grids were performed in different regions of the surface to assess the homogeneity of the results. A force setpoint of 15 nN and approach speed of 1 μm/s were used. Force spectroscopy measurements were carried out at the same temperature as AFM imaging ($T = 25$ °C).

For convenience, let us introduce at this point a description of the typical force spectroscopy signature of a supported lipid bilayer. During a force curve recording, the tip approaches the surface at constant speed and at a given tip-surface distance, it enters in mechanical contact with the lipid layer (see point 1 in Fig. 1). The supported lipid bilayer is then elastically compressed until the tip breaks through it, jumping in contact with the surface (point 2 in Fig. 1). The perforation of the AFM tip manifests as a horizontal discontinuity in the approach force-distance curve. The vertical force at which this discontinuity takes place corresponds to the maximum force the bilayer is able to withstand before breaking and referred to as the breakthrough force (F_b) or yield threshold force [35]. F_b accounts for the strength of the lateral interactions and organization within the lipid bilayer.

3. Results and discussion

3.1. Parameters affecting vesicle adsorption: lipid bilayer phase and surface free energy of chemically and topographically modified solid surfaces

The shape of a vesicle when it adheres to a surface is determined by the interplay of adhesion, bending and stretching, the latter being adhesion-induced. In the case of strong adhesion, one can write a Helfrich free energy F expression of an adsorbed vesicle considering the adhesion energy, the local bending energy term and the stretching energy [36]:

$$F = \frac{1}{2}\kappa \oint (C_1 + C_2 - C_0)^2 dA - WA_c + \Sigma A \quad (1)$$

The first term depends on the local bending modulus κ (assuming that the Gaussian curvature can be ignored when calculating changes in the free energy), on C_1, C_2, and C_0 denoting the two principal curvatures, and the (effective) spontaneous curvature, respectively, and dA being an infinitesimal membrane area element. The second term is the adhesion free energy with W being the strength of adhesion and A_c the contact area of the vesicle and the surface. The last term accounts for the stretching energy with Σ the lateral tension. The energetic competition that defines the vesicle conformation entails the balance between adhesion energy, elastic stretching, and bending of the membrane. In the case of strong adhesion −strong W in Eq. (1)− , the adsorbed vesicle typically adopts the shape of a spherical cap. Thus, the adhesion W can be related to the lateral tension Σ via the Young-Dupré equation $W = \Sigma(1 + \cos\psi_{eff})$, with ψ_{eff} the effective contact angle. Adhesion not only enhances the lateral tension in the membrane but, as shown by Lipowsky and Seifert, increases the rate of vesicle fusion and rupture [36]. The lipid bilayer forming the vesicle is laterally isotropic, the difference between the curvature of the membrane and the spontaneous curvature is small and no shear stress has been considered. For simplicity, the volume V constraint and its corresponding variable, the osmotic pressure ΔP have been not included in Eq. (1). The energy cost for bending and stretching a vesicle depends strongly on its lipid membrane organization, which itself is strongly linked to its phase behavior. The adhesion strength of the solid surface depends on its surface energy, which, according to the Owens, Wendt, Rabel and Kaelble method [37] is a sum of independent components associated with specific interactions.

$$\gamma_{sv} = \gamma_{sv}^{p} + \gamma_{sv}^{d}, \quad (2)$$

where the superscripts p and d stand for polar and dispersive interactions. Details on the calculation of γ_{sv} of the solid surfaces under study are included in the Supplementary Material.

Based on the above exposed, we have evaluated the interplay of solid

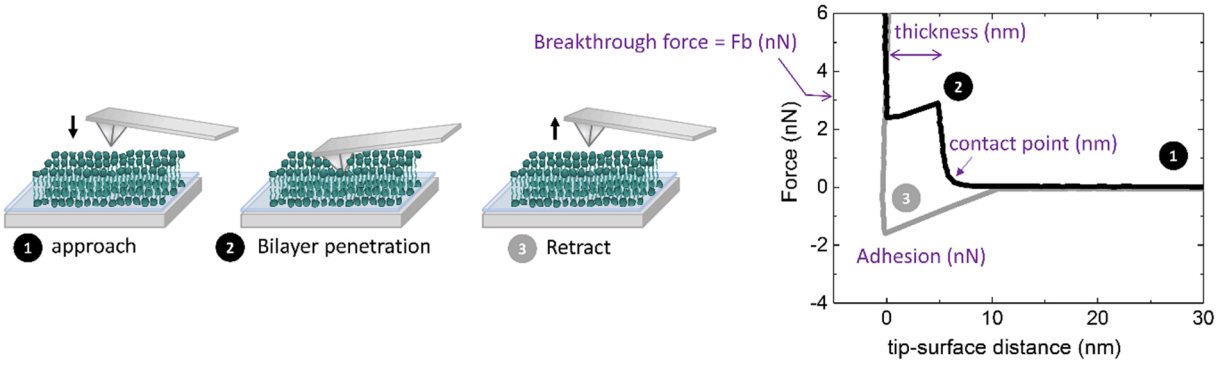

Fig. 1. Force spectroscopy signature of a supported lipid bilayer obtained by AFM, with illustrated schemes of the different steps: 1) the tip approach, 2) the breaking through the bilayer, and 3) the tip retraction.

surface energy and of lipid phase behavior by choosing i) solid surfaces with different degrees of polar component in its surface energy, and ii) lipid vesicles displaying different phases and phase coexistence, respectively. As regards point ii), the area compressibility and the bending elasticity are coupled and both depend strongly on the phase of the lipid bilayer membrane, which in turn depends on temperature [38]. As stated previously, the interplay between the energy gain by adhesion and the cost by bending and stretching an adsorbed vesicle determine its shape and whether it will stay intact or rupture. Therefore, we have chosen to work with DOPC, DPPC and an equimolar mixture of both, which, at the same temperature, display liquid disordered, gel and liquid-gel phase coexistence, respectively. The gel phase exhibits a much larger bending modulus and lower area compressibility modulus than the liquid-disordered phase [38]. In turn, as we shall see later, a system where phase coexistence takes place such DOPC:DPPC vesicles displays intermediate values between the gel and the liquid-disordered phase that scale with the fraction of gel and liquid phase domains [39].

The lipid phase behavior was evaluated by density measurements. Fig. 2A displays the temperature dependence of the specific volume v_L of DPPC, DPPC:DOPC (1:1) and DOPC vesicle dispersions as obtained from density ρ measurements using [40]:

$$v_L = \frac{v_s - (1 - w_L)v_{buffer}}{w_L}, \tag{3}$$

where the subscript L refers to the lipid, $v_s = 1/\rho_s$ is the sample (lipid + buffer) specific volume (inverse of the mass density of the sample ρ_s), v_{buffer} is the specific volume of the buffer $v_{buffer} = 1/\rho_{buffer}$, with ρ_{buffer} obtained from an independent measurement of the density of the pure buffer, and w_L is the mass fraction of lipid in the sample. The molar volumes in Fig. 2A were obtained from specific volumes by $V^m = v_L M$, with M the molar mass of the lipid. Within the studied temperature range (15–45 °C), DOPC is in a homogeneous fluid phase whereas DPPC displays a sharp gel to fluid transition at $T_m = 41.5 \pm 0.1$ °C, reflected in a fast increase of the lipid molar volume. The transition agrees well with previously reported transition values by calorimetry [41]. The equimolar DPPC:DOPC mixture shows a very broad phase transition from gel+fluid coexistence to fluid phase at $T_t = 29.5 \pm 0.5$ °C, in agreement with previously reported transitions obtained by NMR [42]. The polar component of the surface energy of each solid surface used was determined by means of contact angle measurements as described in the Supplementary Material. Fig. 2B shows surface energy values of bare and modified solid surfaces, namely, bare SiO_2, UV-ozoned Au, and Au chemically modified with a homogeneous alkanethiol and with a micropatterned alkanethiol SAM, the latter displaying well-controlled spatial distribution of thiol molecules (see the pattern structure in Fig. 2C and Fig. S1 in the Supplementary Material). The polar contribution to the surface free energy γ_{sv}^p is maximum for SiO_2, followed by UV-ozoned Au, and it is equal to zero for a Au surface homogeneously modified with an alkanethiol SAM in agreement with previously reported values [43,44]. The micropatterned Au surface displays a non-zero value, due to the presence of bare Au surface in between the patterned areas.

3.2. Mechanistic picture of supported lipid membrane formation by QCM-D measurements

Fig. 3 shows the $\Delta f/n$ responses (represented for the third overtone) during DOPC, DPPC and DOPC:DPPC vesicle adsorption on the surfaces under study at 25 °C. The corresponding ΔD responses can be found in Fig. S2 of the Supplementary Material. The observed Δf and ΔD changes are governed by the balance between the energy gain by adhesion which tends to maximize the contact area between the vesicle membrane and the surface and the opposing effect of bending and stretching the bilayer [36].

The mechanistic picture of vesicle adsorption onto SiO_2 varies significantly depending on the phase of the lipid bilayer that forms the vesicle (Fig. 3A). DOPC vesicles in the fluid phase initially adsorb until a critical surface coverage is reached (minimum in Δf and maximum in ΔD), followed by vesicle fusion and rupture leading to $\Delta f = -26 \pm 2$ Hz, in agreement with the formation of a homogeneous rigid and thin SLB, as previously observed in the literature [6,22,45]. The rupture proceeds in bilayer patches with the edges of the patch accelerating the rupture of adjacent vesicles resulting in a homogeneous SLB [46].

For vesicles consisting of the DPPC:DOPC equimolar mixture and

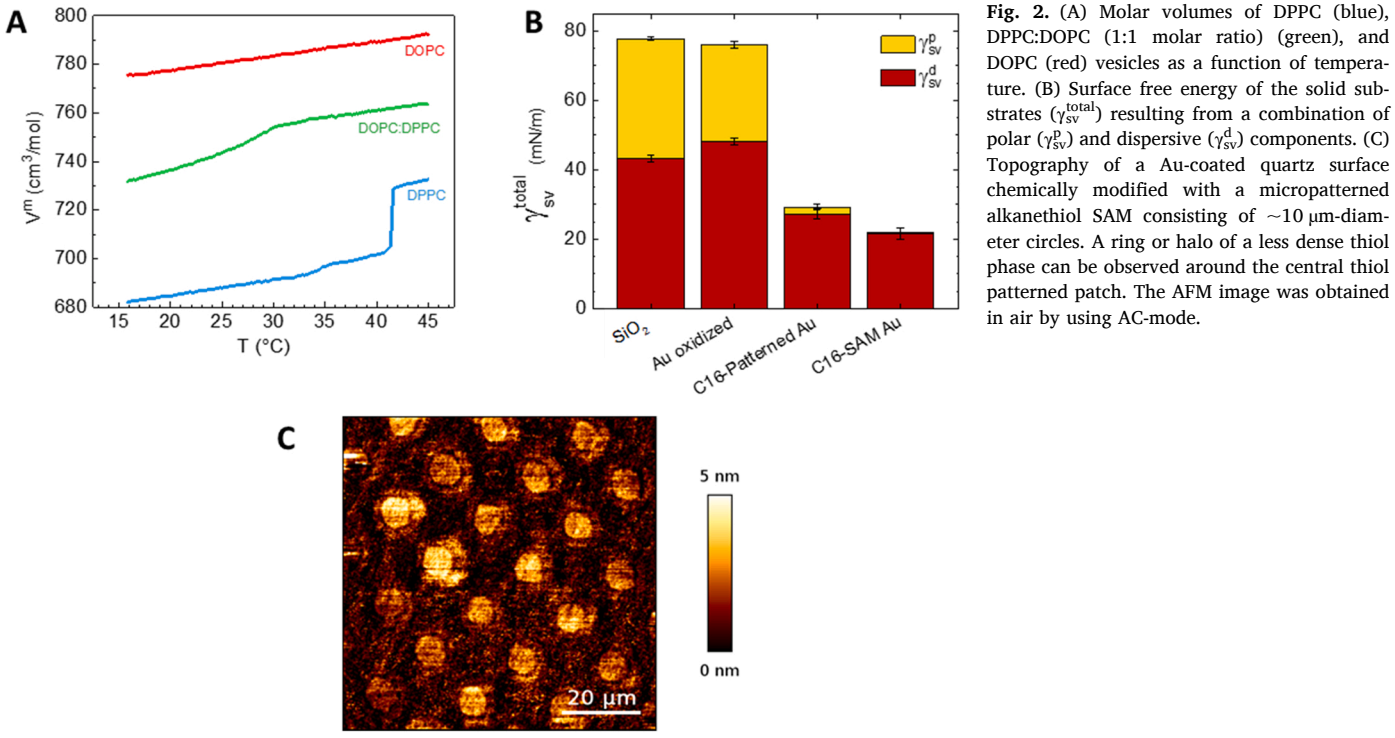

Fig. 2. (A) Molar volumes of DPPC (blue), DPPC:DOPC (1:1 molar ratio) (green), and DOPC (red) vesicles as a function of temperature. (B) Surface free energy of the solid substrates (γ_{sv}^{total}) resulting from a combination of polar (γ_{sv}^p) and dispersive (γ_{sv}^d) components. (C) Topography of a Au-coated quartz surface chemically modified with a micropatterned alkanethiol SAM consisting of ~10 µm-diameter circles. A ring or halo of a less dense thiol phase can be observed around the central thiol patterned patch. The AFM image was obtained in air by using AC-mode.

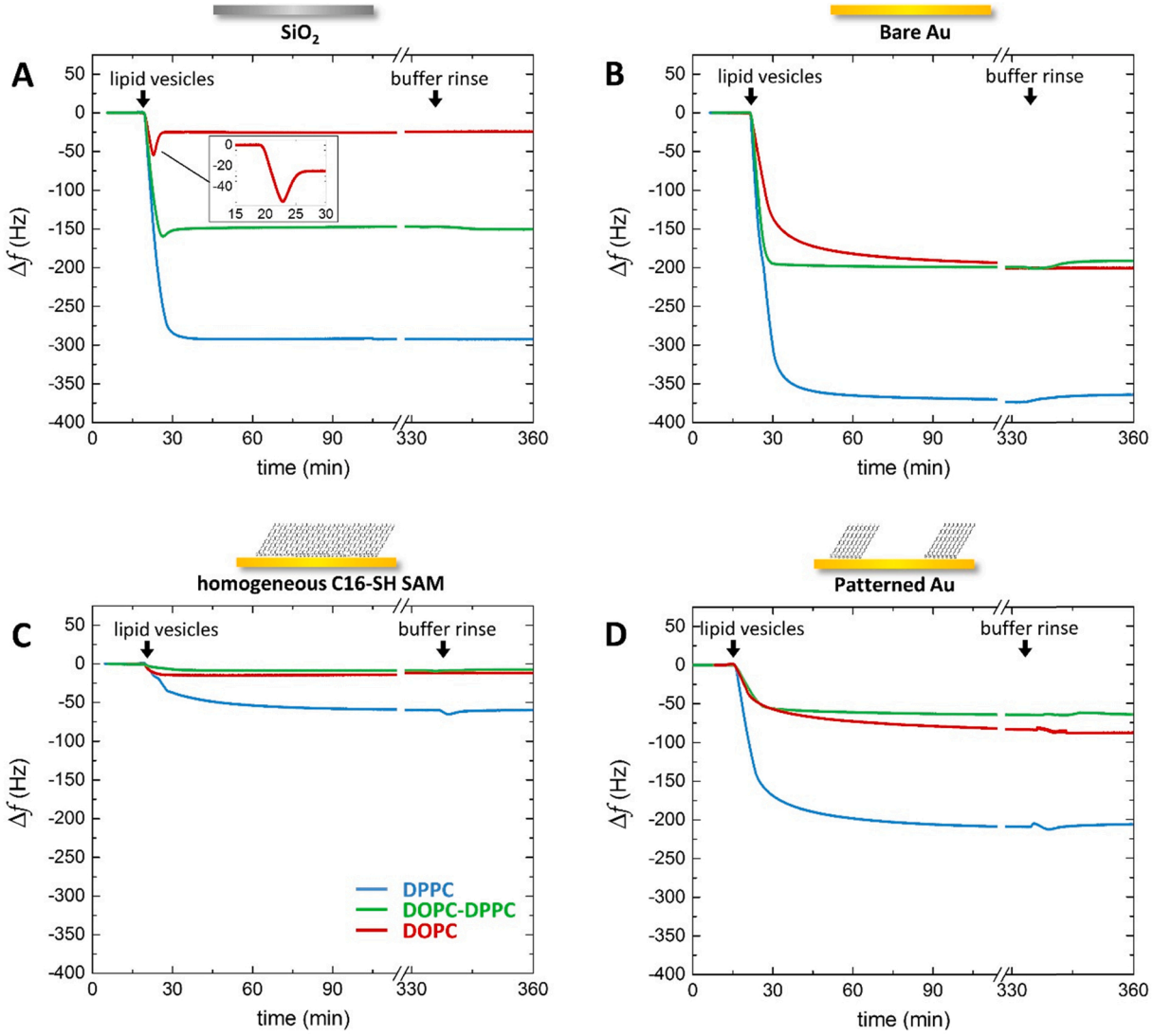

Fig. 3. Frequency shifts observed for the adsorption of DPPC (blue), DOPC (red), and DOPC-DPPC (1:1 molar ratio - green) vesicles on the different surfaces: SiO_2 (A), bare oxidized Au (B), homogeneous C_{16}-SH SAM (C), and patterned Au (D). Vesicle injection as well as buffer rinse times are indicated in the left and right upper parts of each QCM-D plot.

pure DPPC, monotonic frequency and dissipation changes take place reaching constant, non-zero Δf and ΔD plateau values, indicating the formation of an intact, (globally) non-ruptured vesicle layer (see green and blue lines, respectively, in Fig. 3A), as previously reported for DPPC onto SiO_2 [43]. QCM-D is very sensitive to hydrodynamic (wet) mass and the local formation of SLBs cannot be ruled out and might be masked by the adsorption of vesicles on top or in between the bilayer patches [47]. The absolute plateau values are smaller for DOPC:DPPC vesicles than for pure DPPC, the former are softer and more deformable upon adsorption with larger contact area than the latter, yielding a smaller number of vesicles for similar surface coverage. This agrees with predictions of Helfrich and Kozlov and experimental evidence [39,48], where the effective rigidity of a binary lipid mixture can be obtained by the average of the fluid and gel membranes weighted by their respective area fractions, $\frac{1}{\kappa_{eff}} = \frac{\phi}{\kappa_{gel}} + \frac{1-\phi}{\kappa_{fluid}}$, with ϕ the area fraction of the gel phase and κ the bending modulus [39]. For DOPC: DPPC vesicles displaying phase coexistence, the effective rigidity should be closer to pure DOPC than to pure DPPC. On SiO_2 surfaces, DOPC:DPPC vesicle deposition shows a minimum in frequency, however, despite the very high polar contribution to the adhesion energy of SiO_2, the presence of the gel phase (either pure or in macroscopic domains) hinders the global rupture of adsorbed vesicles and the formation of a homogeneous SLB. When adsorbed onto UV-ozoned Au, larger Δf and ΔD plateau values are obtained for all three types of vesicles as compared to SiO_2 surface counterparts (see Figs. 3A and 3B for Δf plateaus and Figs. S2A and S2B in the Supplementary Material). This agrees with the fact that larger Δf and ΔD plateau values for the same system when adsorbing onto bare Au as compared to SiO_2 have been previously observed in the literature (see Refs. [22,43]).

The adsorption behavior onto a Au surface with a 1-hexadecanethiol SAM (formed by overnight immersion of the surface in a ethanolic solution of the thiol molecules) follows a monotonic behavior for both DOPC and DOPC:DPPC vesicles (see red and green lines in Fig. 3C). The plateau values $\Delta f = -11 \pm 1$ and -8 ± 1 Hz lies very close, although slightly below half the value obtained for a homogeneous SLB, as previously observed for eggPC and DMPC lipids [22,23]. The values of $\Delta D = 1.1 \pm 0.5$ and $0.7 \pm 0.4 \times 10^{-6}$ obtained indicate the formation of a hybrid bilayer (lipid monolayer on top of the SAM) with probably some defects as it will be discussed later. The driving force for hybrid bilayer formation is the hydrophobic interaction between the bilayer and the SAM layer, and takes place in several steps. First, a hemifusion neck is formed between the bilayer and the hydrophobic SAM, which might either remain stable or lead to vesicle collapse by unzipping of the two

leaflets [23]. The fate of the hemifused vesicle depends thus on energy required for rupturing the bilayer and unzipping. QCM-D responses reveal that DPPC vesicles adsorbed on homogeneous 1-hexadecanethiol SAM do not form homogeneous hybrid bilayers judging from the large Δf and ΔD values obtained (blue line in Fig. 3C). In this case, local rupture might have occurred together with adsorbed hemifused DPPC vesicles.

When adsorbed onto alkanethiol-micropatterned Au surfaces, Δf and ΔD exhibit intermediate plateau values between those obtained for bare Au and homogeneously-coated SAM Au (see Fig. 3D). This might be expected given the presence of micrometer-sized bare Au areas in between alkanethiol-patterned patches. Most likely, when vesicles diffuse to the surface, they might preferentially adsorb either on bare or thiol-covered Au. In this context, atomic force microscopy serves as a useful tool to unravel the topography and the nanomechanical properties of the formed layer as shall be confirmed in Section 4 of this manuscript.

The thickness of the resulting supported membranes has been calculated using a Kelvin-Voigt-based viscoelastic model using data from overtones 3rd to 11th and keeping as fixed parameters the density of the lipid layer 1.06 g/cm^3, the density and the viscosity of the aqueous buffer 1.0 g/cm^3 and 1 mPa s, respectively. Although the model assumes that the layer is homogeneous, it can still provide a qualitative idea of QCM-D type of layer formed. Fig. 4 provides a 3D-overview of the correlation among the polar component of the surface energy, the thickness of the resulting layers and the frequency plateau data for all three types of lipid systems. This diagram helps to classify the type of layers obtained into homogeneous hybrid bilayers, homogeneous supported lipid bilayers, inhomogeneous intact vesicle/patch and supported lipid vesicles. The dissipation analogue is included in Fig. S3 of the Supplementary Material.

The formation of homogeneous layers can be distinguished at the surfaces with largest and smallest polar components, SiO_2 (squares), and homogeneously SAM-modified Au surface (triangles), respectively. On both types of surfaces, adsorption of DOPC vesicles (red symbols) yields very thin and quite homogeneous layers, namely lipid bilayers and hybrid bilayers. This confirms that lipid vesicles in the liquid disordered phase are quite deformable and can rupture onto surfaces with opposite surface energy. On SiO_2, rupture is mediated by vesicle fusion upon adhering and subsequent rupture due to strong interactions between the hydrophilic head group and the hydrophilic surface. On the SAM-modified Au surface, rupture is mediated by hydrophobic interactions between the hydrophobic core of the bilayer and the alkyl chain of the

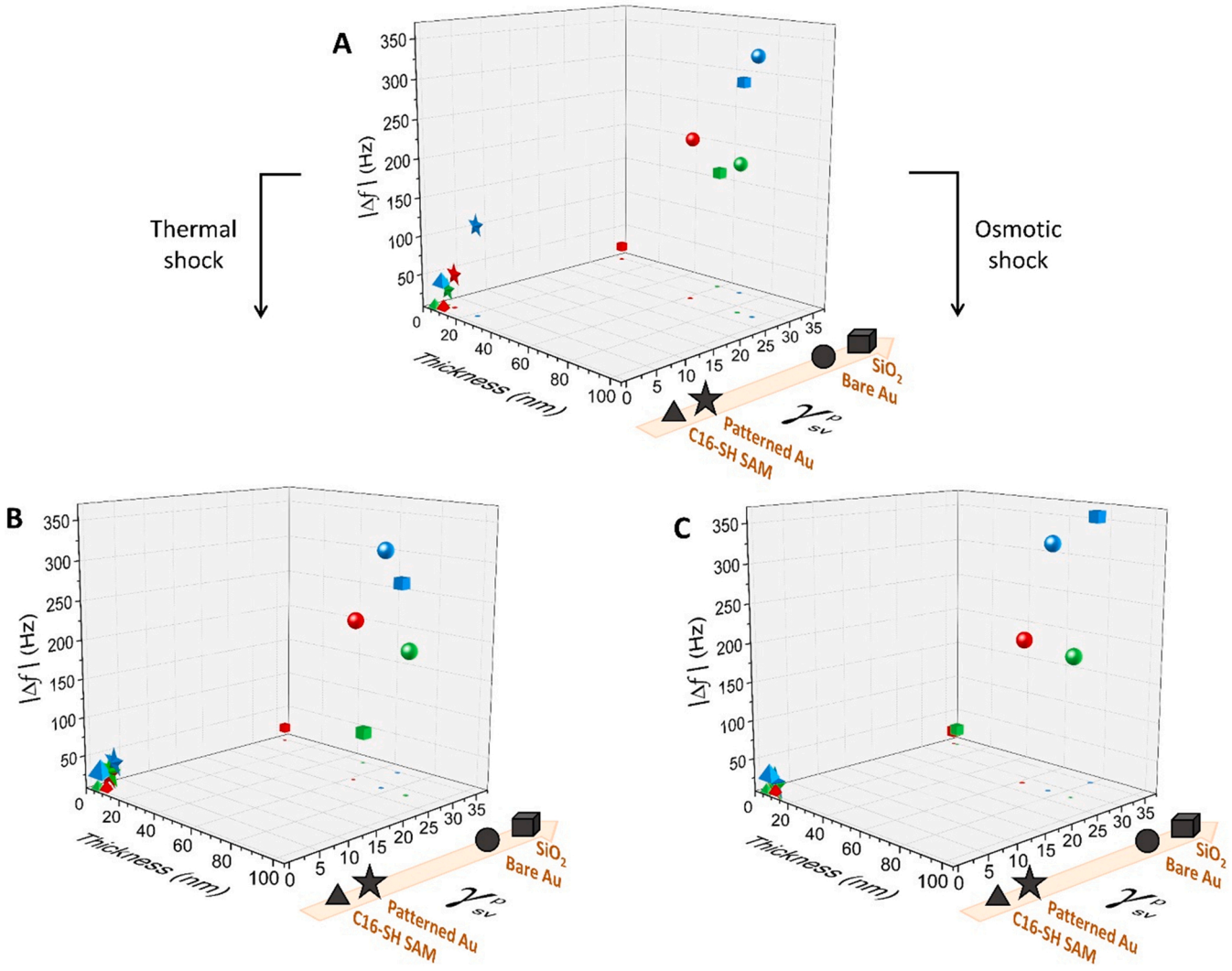

Fig. 4. 3D-view of the supported lipid layer properties after vesicle adsorption (A), and after a thermal shock (B) or an osmotic shock (C). Geometrical figures stand for the different surfaces used and their corresponding polar component of the surface energy. SiO_2 as cubes, spheres as bare Au, stars as SAM-patterned surfaces and triangles as Au surfaces homogeneously coated with a SAM layer. The colors refer to the type of lipid used (DPPC = blue symbols, DPPC:DOPC = green symbols, DOPC = red symbols), associated with the resulting thickness of the adsorbed lipid layers.

SAM. Adsorption of binary DOPC:DPPC vesicles (green symbols) leads to homogeneous hybrid bilayers onto SAM-modified surfaces, whereas it leads to supported vesicle layers (SVLs) on SiO_2. The presence of gel domains in the DOPC:DPPC lipid mixture makes the adhesion strength of the SiO_2 surface insufficient to induce global rupture. In turn, hydrophobic interactions are large enough to promote the unzipping of the vesicle bilayers and spreading into hybrid bilayers. For DPPC vesicles (blue symbols), no global rupture occurs onto SiO_2, and a partial one occurs onto homogeneous SAM-modified Au surfaces. DPPC layers on SiO_2 can be considered as SVLs, while on homogeneous SAM-modified Au surface hemifused vesicles do not fully spread over the surface, yielding very inhomogeneous effective layer thicknesses ($h = 68 \pm 23$ nm vs $h = 92 \pm 7$ nm for non-ruptured vesicles on bare Au surfaces). In fact, a homogeneous DPPC hybrid layer can be formed by increasing the vesicle injection time (see Fig. S4 in the Supplementary Material). Increasing exposure time yields a larger vesicle coverage and destabilizes hemifused vesicle thus enabling easier spreading.

On bare Au (circles), all three types of lipid vesicles display large frequency and thickness values upon adsorption pointing towards the formation of intact vesicle layers. On alkanethiol-patterned Au surfaces (stars), values are typical from mixed layers: the shifts in frequency are quite small, indicating some rupture, but the global thicknesses comprised between 10 and 20 nm are representative from inhomogeneous layers with the presence of unruptured vesicles.

Furthermore, Fig. 4 shows the stability of the formed supported lipid membranes from a two-fold point of view, i) by performing cyclic thermal scans at a fixed heating/cooling rate (panel B) and ii) by rinsing the formed layers with DI water and thus inducing an osmotic change (panel C). An analogue diagram for the dissipation changes is included in Fig. S3 of the Supplementary Material. Vesicles adsorbed on Au surfaces (spheres) form stable SVL systems since no changes in the layers are observed upon both thermal and osmotic shocks for all three types of lipids. On SiO_2 (cubes), vesicles are supposed to deform more, thus they are expected to be less stable, which is the case of DPPC:DOPC SVLs, where a homogeneous bilayer can be directly obtained right after a water rinse, whereas 70% of the vesicles rupture upon a thermal shock. DPPC being more rigid, the layers tend to be less affected by these external stimuli. Indeed, the heating/cooling cycle induces only a slight decrease in frequency with no significant changes in dissipation nor in thickness, showing that few of the vesicles ruptured without changing the global organization of the SVL. Interestingly, upon the osmotic shock, a decrease of frequency and an increase of dissipation of 23% and 25%, respectively, are observed and can be related to structural changes within the vesicle layer.

Additional information regarding the type of layer formed on the different surfaces can be obtained from the phase transition profiles of the adsorbed layers as displayed in Fig. 5. These profiles were obtained by performing thermal scans from 16° to 50°C with QCM-D, after the adsorption of the lipid layers at 25 °C. During the thermal scans, DPPC (panel A) and DPPC:DOPC (panel B) layers underwent their main transition, which reflects as maxima in the first-order temperature derivative of the frequency $d\Delta f/dT$ for all overtones (minima in the dissipation temperature derivative $d\Delta D/dT$) [49,50]. In contrast, DOPC lipid layers did not display any phase transition, since the melting temperature of the lipid lies well below the studied temperature range, as shown in Fig. S5. A recent study showed that the shape of the transition peak depends on the degree of deformation of the lipid vesicle upon adhesion to the surface [50]. For vesicles adhered on bare Au, the transition peak and transition temperatures ($T_m = 42.1 \pm 0.3$ °C and $T_m = 30 \pm 1$ °C for DPPC and DPPC:DOPC, respectively) agree well with what is observed in bulk systems from density measurements ($T_m = 41.5 \pm 0.1$ °C and $T_m = 29.5 \pm 0.5$ °C) and previously reported transitions by calorimetry [42], indicating that on bare Au vesicles remain rather intact.

Conversely, on SiO_2, the transition peaks are very intense, and shifted to higher temperatures. This corresponds to a larger vesicle deformation and contact area to the SiO_2 surface, which results in a clear decoupled melting for DPPC vesicles in agreement with previously reported results [43], the first one occurring at $T_m = 41.5 \pm 0.8$ °C, in the same range as for Au surfaces, and the second one occurring later at $T_m = 44.8 \pm 0.4$ °C. As previously reported [43], adsorbing vesicles at $T < T_m$ favour the gel phase of lipids in the adhered part of the vesicle membrane. For DOPC:DPPC vesicles, the transition is shifted to higher temperatures as compared to bulk, clearly indicating lipid phase reorganization due to the presence of the solid surface. For chemically and topographically alkanethiol modified surfaces, only the transition in adsorbed DPPC vesicles is detectable, which is due to unruptured, hemifused vesicles adsorbed on the thiol layers (smaller peak intensity thus smaller number of intact vesicles). For DPPC:DOPC vesicles, no transition is observed which points towards the fact that quite some rupture (more efficient rupture than in Au) took place in these surfaces.

3.3. AFM characterization of the supported lipid membranes

The topographical characterization of supported lipid layers was carried out in HEPES buffer solution using Quantitative imaging mode (QI), and the nanomechanical properties of the layers were determined by force spectroscopy, from which characteristic force-distance curves can be obtained. Force spectroscopy measurements were carried out

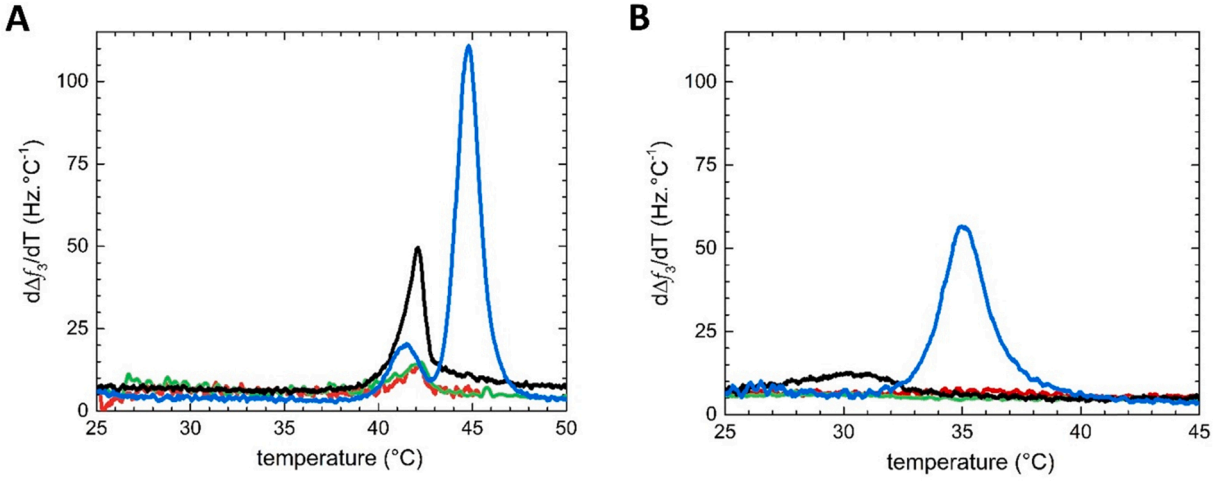

Fig. 5. Dependence of main phase transition of adsorbed vesicles on the nature of the underlying substrate, namely, bare oxidized Au (black), patterned Au (green), homogeneous C_{16}-SH SAM (red), and SiO_2 (blue). $d\Delta f_3/dT$ curves obtained upon heating demonstrate the phase transitions of DPPC (A) and DPPC:DOPC (B).

using arrays of 16 × 16 points, obtaining 256 force curves per measurement. As it will be shown in the following subsections, AFM measurements helped unravel the topography of the formed layers on the different surfaces, confirming the QCM-D results displayed in Fig. 4. In addition, the nanomechanical signatures provided information on the layer stability. In what follows, results will be presented by the type of surface used, namely SiO_2, bare Au, 1-hexadecanethiol SAM-modified Au by immersion, and 1-hexadecanethiol micro-patterned Au. All the results shown below come from lipid films that were prepared according to the ex-situ procedure, as explained in the Section 2.8. This approach allows to form the lipid films directly in the AFM liquid cell and minimizes the risk of dewetting.

3.3.1. *Topographic and nanomechanical characterization on SiO_2*

Supported lipid bilayers were obtained from the global rupture of DOPC and DOPC:DPPC vesicles on SiO_2 wafers after a surface immersion into the lipid solutions for 30 min. At room temperature, the DOPC SLB is very homogeneous (panel A in Fig. 6), with an RMS roughness $R_q = 0.3 \pm 0.1$ nm (see the cross-section of panel D in Fig. 6). The lipid film thickness obtained from the layer penetration is $h = 4.8 \pm 0.2$ nm and breakthrough force $F_b = 2.8 \pm 0.7$ nN (panel G in Fig. 6). These values agree very well with previously reported thickness and F_b of DOPC in water or DPBS buffer on mica surfaces [35,51]. The DOPC: DPPC SLB displays clear phase separation between gel and liquid disordered domains (panel B in Fig. 6). The difference in thickness between the two coexisting phases is $\Delta h \sim 1.0 \pm 0.1$ nm, (panel E in Fig. 6), in agreement with previously reported values of DOPC:DPPC onto mica surfaces [52]. The presence of macroscopic phase separation is also reflected in force spectroscopy measurements, with well-differentiated breakthrough force values between gel phase domains (DPPC-rich) and liquid disordered domains (DOPC-rich) (see panel H in Fig. 6). The formation of SLBs displaying phase separation differs from the DOPC:DPPC layers (mainly SVLs) obtained on SiO_2-coated quartz sensors using QCM-D (in Fig. 3A). Fig. S6 shows a comparison between the DOPC:DPPC layers formed on both SiO_2 wafers and SiO_2-coated quartz sensors: a SLB for the first one, and a SVL for the second one. The reasons behind this apparent discrepancy can be attributed to the fact that at the working adsorption temperature, the difference in roughness of the surfaces ($R_q = 0.13 \pm 0.02$ nm for the wafers vs 1.12 ± 0.09 nm for the quartz crystals) can affect the lipid adsorption. Further details on the effect of surface roughness will be provided in a different publication.

DPPC vesicles in the gel phase did not (globally) rupture as can be inferred from the intact structures with thickness $h = 42 \pm 9$ nm and lateral size of 133 ± 10 nm (panels C and F in Fig. 6). The associated force curve shown in panel I differs significantly from the one observed for an SLB and indicates that the tip is compressing a vesicle [53]. The contact point with the vesicle starts at a tip-sample distance of $d = 45 \pm 10$ nm, when the tip starts compressing the adsorbed vesicle. A first jump-in takes place at 20 nm, which corresponds to the tip breaking through the bilayer of the vesicle at the vesicle-buffer interface. This is

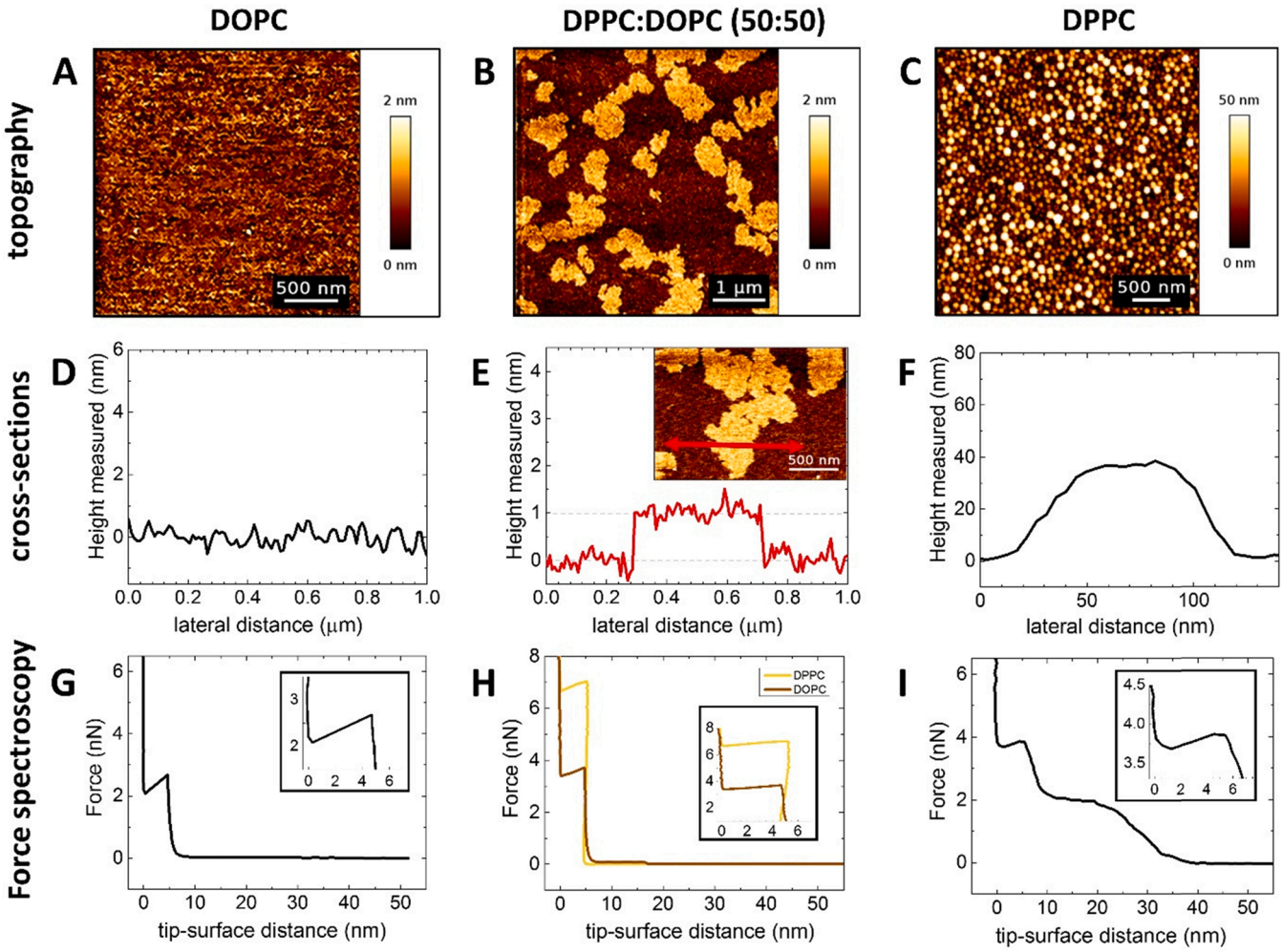

Fig. 6. AFM topographical images, cross-sections, and force curves obtained from force spectroscopy measurements of DOPC (A, D, G), DPPC:DOPC (50:50) (B, E, H) and DPPC (C, F, I) vesicles adsorbed on SiO_2 wafer. QI and force spectroscopy measurements were carried out in HEPES buffer at room temperature. The force curves shown, are representative from the average number of curves used in the statistical analysis. On panel E, the red arrow illustrates the location of the cross-section.

followed by subsequent compression and a second jump-in at 5 nm, when the bilayer in contact with the SiO_2 surface is perforated.

Average breakthrough force values and thickness of SLBs and contact point values for vesicles can be found in Table S1 in the Supplementary Material. Figures displaying histograms of breakthrough force, thickness and contact point are included in Fig. S7 together with the number of curves used in each histogram.

3.3.2. Topographic and nanomechanical characterization on bare Au

On bare Au no global rupture was observed for any of the three types of lipid systems used. Yet, differences in vesicle deformation upon adsorption due to the different lipid phases are clear. Fig. 7 shows the correlation between lipid phase and vesicle deformation. DOPC vesicles in the liquid disordered phase show the largest deformation, followed by DOPC:DPPC vesicles, which bear macroscopic phase separation, and DPPC vesicles adsorbed at the gel phase. The vesicle thickness of the vesicle layers was estimated from cross-section (see panels D, E, and F), h (DOPC) $= 17 \pm 5$ nm, h (DOPC:DPPC) $= 40 \pm 7$ nm, and h (DPPC) $= 76 \pm 10$ nm, respectively. These values agree quite well with the contact points of the force curves d (DOPC) $= 19 \pm 3$ nm, d (DOPC:DPPC) $= 51 \pm 8$ nm, and d (DPPC) $= 65 \pm 23$ nm, (see panels G, H, and I of Fig. 7, and Fig. S7 and Table S1 in the Supplementary Material). As for the case of DPPC vesicles adsorbed on SiO_2, the observed thickness are lower than the effective thickness values obtained by QCM-D using a viscoelastic model (h (DOPC) $= 62 \pm 5$ nm, h (DOPC:DPPC) $= 85 \pm 5$, and h (DPPC) $= 92 \pm 7$ nm). This difference stems from several factors. During AFM imaging, vesicles are compressed, thus thickness values are underestimated. On the other hand, the viscoelastic model used in QCM-D assumes that the layers are fully homogeneous, which, as observed from AFM images, is not the case –especially for DOPC layers where both supported lipid bilayers and deformed vesicles coexist–, and thickness values are overestimated.

3.3.3. Topographic and nanomechanical characterization on a 1-hexadecanethiol SAM-modified Au

Macroscopically, the SAM-modified surfaces are very hydrophobic, i.e., water contact angle $= 108 \pm 1°$, however, the packing and lateral organization of the SAM at a microscopic level depends strongly on the topography and presence of defects of the underlying Au surface [28]. For AFM measurements involving SAMs, ultraflat Au wafers ($R_q = 0.56 \pm 0.08$ nm) were used, (see Fig. S8 of the Supplementary Material). The RMS roughness of the SAM-modified Au surfaces are $R_q = 0.97 \pm 0.18$ nm. The exposure of DOPC and DOPC:DPPC vesicles on the 1-hexadecanethiol SAM-modified Au surface, leads to layers with similar topography (see panels A and B of Fig. 8) and rather large RMS roughness values of R_q (DOPC) $= 1.05 \pm 0.09$ nm and R_q (DOPC:DPPC) $= 1.7 \pm 0.6$ nm (panels D and E). Due to the presence of few defects (holes in the membranes), we can estimate the hybrid layers thicknesses (see one example with the green arrow in panel E for the DPPC:DOPC case, where the layer thickness is $h = 4.9 \pm 0.3$ nm). Upon exposure to DPPC vesicles, global rupture takes place, however lipid spreading is not completely efficient and supported hybrid bilayer patches can be observed (panel C). The thickness values of the patches determined by cross-sections are about $h = 2.4 \pm 0.2$ nm, which are consistent with

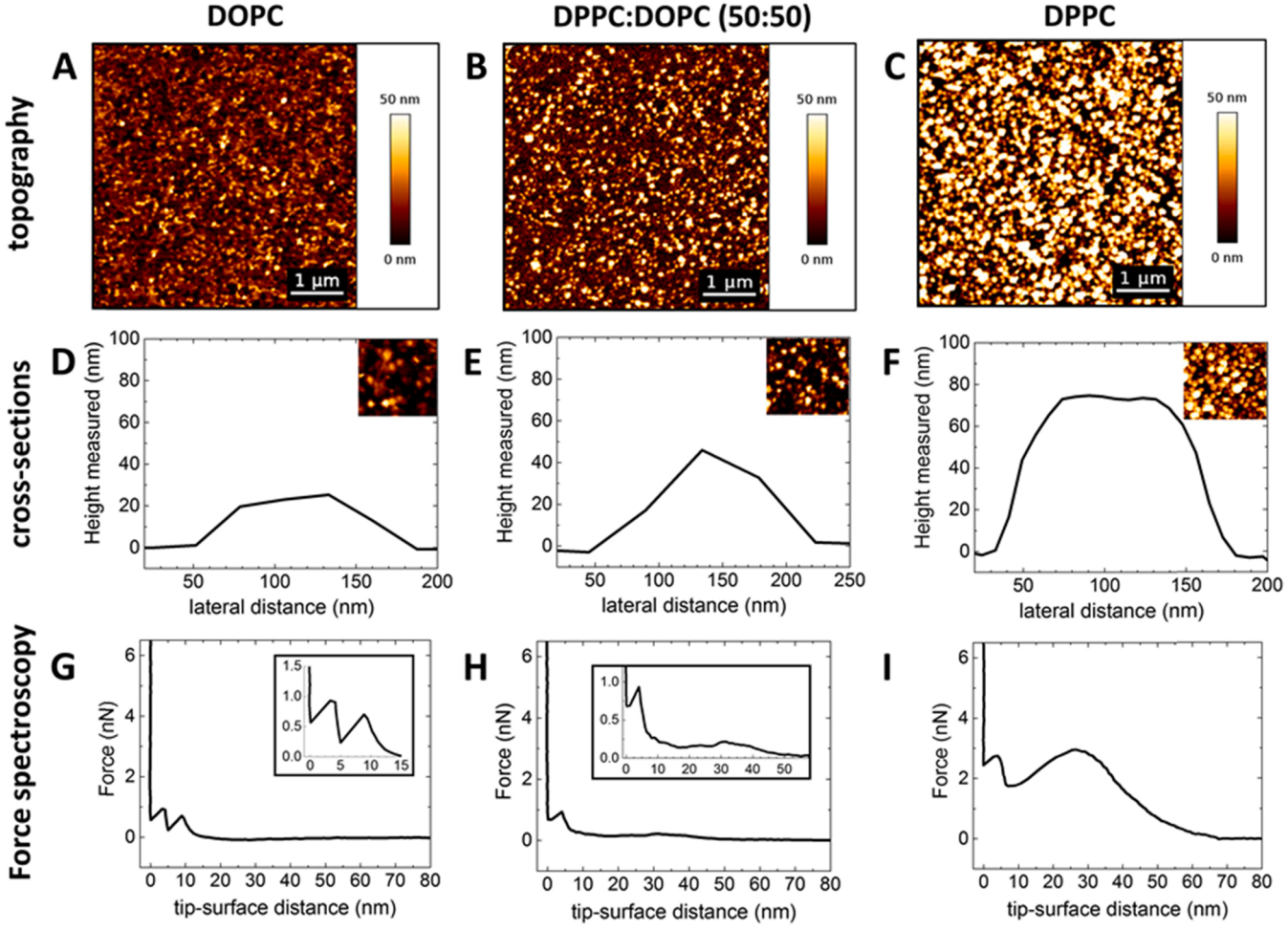

Fig. 7. AFM topographical images, cross-sections, and force curves emanating from force spectroscopy measurements of DOPC (A, D, G), DPPC:DOPC (50:50) (B, E, H) and DPPC (C, F, I) vesicles adsorbed on bare Au. QI and force spectroscopy measurements were carried out in HEPES buffer at room temperature.

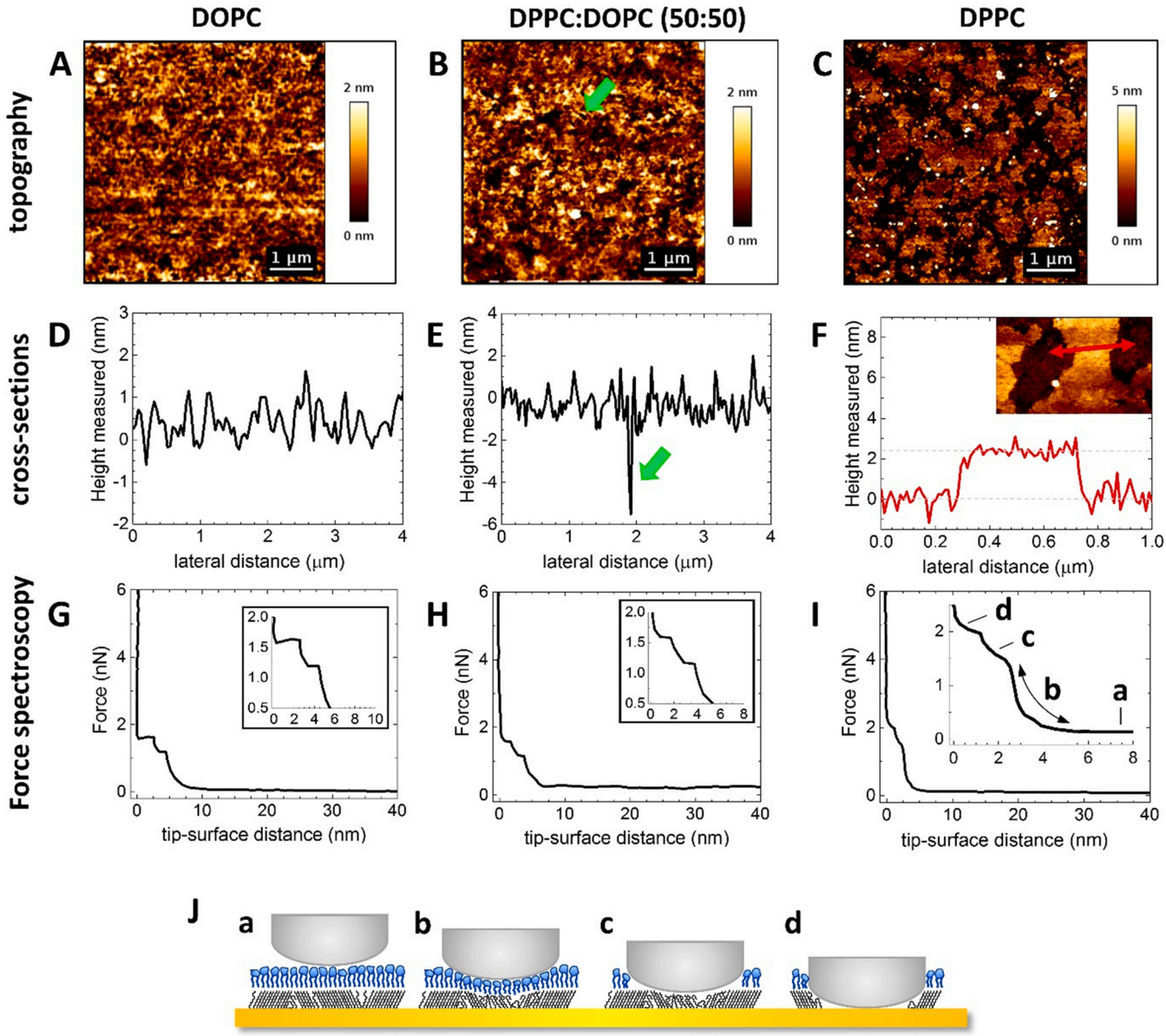

Fig. 8. AFM topographical images, cross-sections, and force curves from force spectroscopy measurements of DOPC (A, D, G), DPPC:DOPC (50:50) (B, E, H) and DPPC (C, F, I) vesicles adsorbed on C16-alkanethiol SAM. QI measurements were carried out in HEPES buffer at room temperature. Panel J is an illustration of the hybrid layer perforation performed by the tip. Each event (labels a to d) is reported in panel I, but it is also valid for the two other force curves shown.

lipid monolayers (see panel F). The spreading of the lipid being difficult, some hemifused DPPC vesicles are also observed on the QI image (white spots). According to their level of hemifusion, they are characterized by thickness values ranging from h = 8–35 nm (most of them being between 10 and 15 nm). For all the three types of hybrid layers, the force curves seem to be decoupled into two jumps (panels G, H, and I), which indicate that the tip perforates sequentially the upper (lipid) and the lower (SAM) leaflets. Contrary to the SLBs formed on SiO_2, for which clear jumps appear in all force-distance curves all over the sample, the frequency of force curves displaying jumps in hybrid supported SAM/-lipid bilayers is smaller and inhomogeneous over the surface. In less compact areas, the poor packing and lateral organization of the bilayers lead to an absence of jumps in the force curves, which reflects a poor packing within the lipid membrane [54], and represents in our case an important part of the curves in the force maps (60%, 35%, and 44% of the force curves for DOPC, DPPC:DOPC, and DPPC surfaces respectively). The number of maps used to produce the histograms shown in Fig. S7 was larger to keep a consistent amount of exploitable force curves. Thickness values extracted from force spectroscopy experiments and shown in Table S1 ($h = 3.3 \pm 0.6$ nm for DOPC, $h = 2.9 \pm 0.5$ nm for DOPC:DPPC, and $h = 3.8 \pm 0.7$ nm for DPPC) are smaller than standard SLBs. This can be explained due to the absence of the underlying water layer in contact with the surface. The contact point values (the distance from the surface where repulsive contact between the AFM tip and the layer starts) stay in the range of 4.9–5.5 nm.

3.3.4. Topographic and nanomechanical characterization on a 1-hexadecanethiol patterned-modified Au

Fig. 9A shows a sketch of an alkanethiol SAM-patterned Au surface, which, ideally, is divided into two regions, namely, the area covered by the PDMS stamp −with patterned circles (1) and non-patterned areas between the circles (2)− and the area uncovered by the PDMS stamp (bare Au). We have included as example DPPC layers formed on alkanethiol-patterned Au-surfaces. Outside the area covered by the PDMS stamp on bare Au, large intact vesicles of thickness of 73 ± 10 nm can be observed (see panel B4 in Fig. 9). Inside the SAM printed patches,

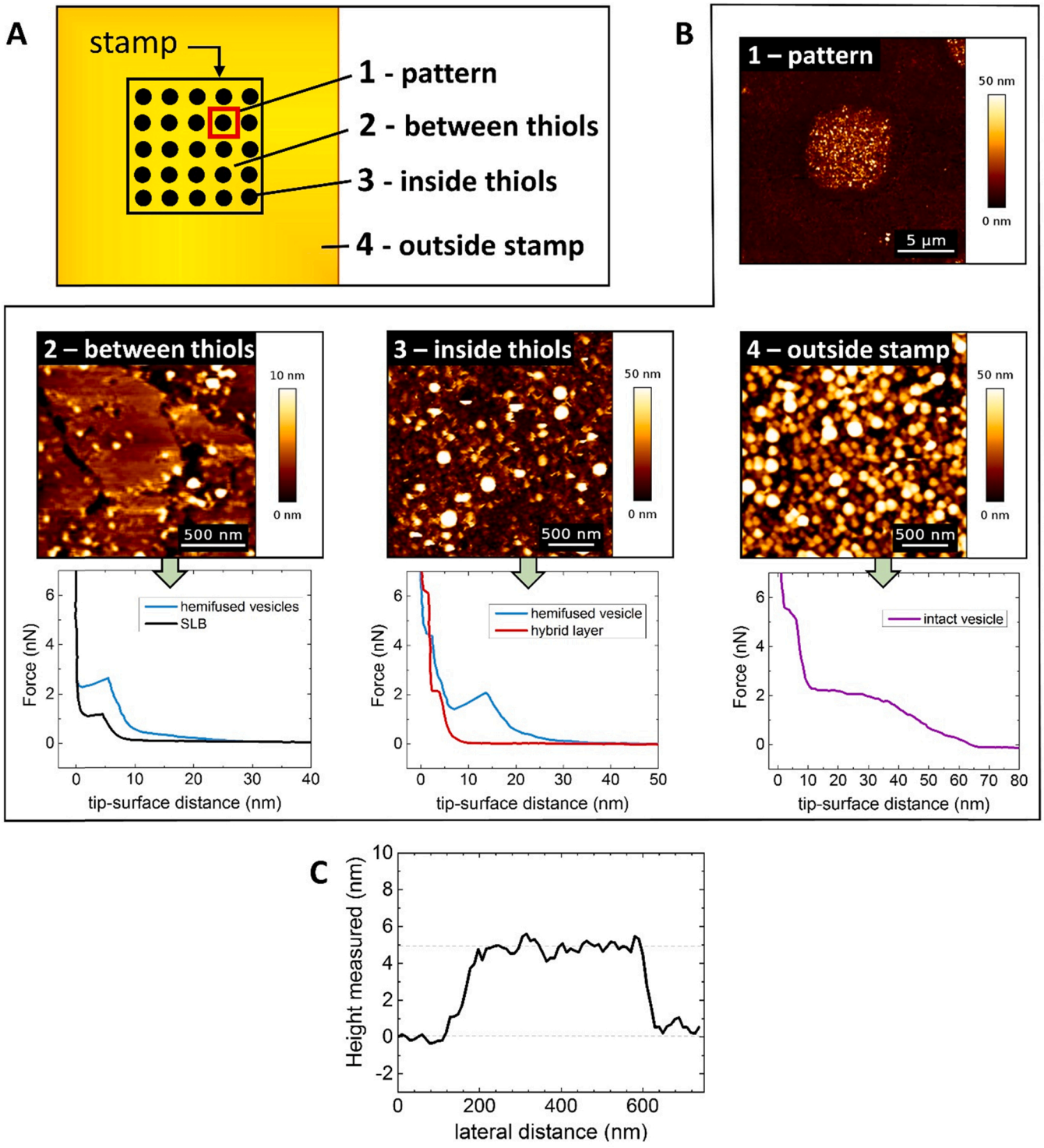

Fig. 9. Structure of a patterned surface (A) with (B) the associated AFM topographical images and force curves of DPPC in the specific regions studied: an entire thiol disk (1), the space between the disks (2), a focus on the inside of the thiol disk (3), and the bare Au situated outside the stamp (4). QI measurements and force spectroscopy measurements were carried out in HEPES buffer at room temperature. Panel C is a cross-section of the patches shown in panel B2.

a quite inhomogeneous distribution of hybrid thiol/lipid bilayers and unruptured, hemifused vesicles onto the SAM print can be seen (see panel B3 in Fig. 9). The halo surrounding the SAM patterned core circle and acting as a boundary between patterned and non-patterned regions appears darker in the AFM image, indicating that no vesicle adsorption takes place in that region. Along the halo, thiol molecules bear a different orientation with a less dense packing [33]. In a previous report involving eggPC vesicles adsorbing on micropatterned hybrophobic/hydrophilic regions, the boundary region was shown to play and important role acting as nucleation site for vesicle rupture and bilayer growth [55]. In between the SAM prints, a smaller amount of vesicles was observed as compared to bare Au regions non exposed to the PDMS stamp. Instead, patches of thickness ~ 5 nm can be detected, indicating local vesicle rupture (see panels B2 and C in Fig. 9). A similar behavior was observed on thiol-patterned Au surfaces exposed to DOPC: a global vesicle rupture inside the patterned core (DOPC bilayers being

fluid at room temperature) and supported lipid bilayers in between the patterns (see Fig. S9 in supplementary information). The presence of supported lipid bilayers on out-of-printed regions which are supposed to be SAM-free reflects the influence of imprinting in the neighboring areas, which has been experimentally shown in recent works involving corrosion inhibition of metallic surfaces using microcontact printing of alkanethiol and thiol-based molecules [56,57]. The corresponding force curves recorded in the above-described regions are consistent with the variety of structures observed, namely hybrid bilayers, lipid bilayers and hemifused vesicles.

4. Conclusions

We have evaluated the interplay between lipid bilayer phases and solid support surface energy and topography in modulating the formation and stability of supported lipid bilayers including hybrid leaflets. Our study highlights the need for complementary multiscale techniques to provide a complete picture of the formed supported membranes.

Real time QCM-D measurements have provided a mechanistic overview of vesicle adsorption and rupture, highlighting the effect of the lipid phase and polar contribution to the surface energy. On surfaces with very large or very low polar component, i.e., SiO_2 and SAM-modified Au by immersion, the lipid phase plays a decisive role in the quality of the bilayers formed. Thus, vesicles in the liquid phase or vesicles displaying phase separation between liquid and gel phases rupture and spread easily leading to homogeneous lipid bilayers on both SiO_2 and hybrid bilayers on SAM-modified Au. Most of the vesicles in the gel phase remain intact or hemifused to the SAM layer and only local rupture takes place, owing to larger activation energies involved and less efficient lipid spreading. SAM-modified surfaces are very sensitive to lipid vesicle injection time, the longer the injection, the larger the vesicle coverage, leading to an easier rupture of hemifused vesicles and subsequent spreading into hybrid bilayers.

AFM imaging confirmed for most of the cases the topography (lateral and vertical) of the formed supported membranes predicted by QCM-D results. Nanomechanical mapping revealed significant differences between supported lipid bilayers on SiO_2 and hybrid bilayers on SAM-modified Au. Supported lipid bilayers on SiO_2 display clear, single jump, discontinuities in the approach force distance curves, which account for a well-organized and stable lipid bilayer. Hybrid bilayers exhibit a weaker nanomechanical stability, with less frequent force curves displaying double jumps and suggesting decoupling between the upper lipid and lower SAM leaflet when vertically compressed at a constant speed.

The adsorption of lipid vesicles onto Au surfaces microcontact printed with well-localized SAM patterns shows QCM-D intermediate responses between those observed on bare, unmodified Au and homogeneously SAM-modified Au surfaces. Thermal and osmotic shocks lead to quite homogeneous layers with very small dissipation values. AFM was particularly useful to reveal the actual distribution of lipids on the core patterned SAMs and on the non-patterned Au regions in between the SAM patterned core. Full rupture is observed on top of the SAM imprints for lipids in the liquid phase, while lipids in the gel phase hemifused vesicles remain. Surprisingly, in between the SAM imprinted circles, patches commensurate with the thickness of a bilayer were observed, instead of intact vesicles. The spatial control of the supported lipid structure (hybrid bilayers or pure bilayers) and the layer mechanical properties in a unique solid support by using a straightforward one-step surface modification, is a step towards the design of lipid-based platforms for mechanosensitive studies. Further fundamental research would be needed to unravel how patterning impacts the surrounding surface and the role of the domains separating the patterned regions.

CRediT authorship contribution statement

L. Bar: Microcontact printing, QCM-D, DLS, AFM data acquisition, analysis, and editing, **M.E. Villanueva**: density, QCM-D data acquisition, analysis and editing, **C. Martín**: QCM-D and contact angle data acquisition analysis, reviewing, editing, and fund raising **A. Valencia-Ramírez**: microcontact printing, editing **J. Goole**: DLS data acquisition and methodology, **F.U. Renner:** conceptualization, editing, and fund raising. **P. Losada-Pérez**: conceptualization, supervision, writing, reviewing, editing and fund raising.

Declaration of Competing Interest

The authors declare the following financial interests/personal relationships which may be considered as potential competing interests: Patricia Losada Perez reports financial support was provided by FNRS. Patricia losada perez reports a relationship with FNRS that includes: funding grants. not applicable.

Data Availability

Data will be made available on request.

Acknowledgements

P.L.P. acknowledges MIS and HTMSoft projects 40003040 and 40008129 by 'Fonds de la Recherche Scientifique' (FNRS). A.V.R. and F. U.R. thank Prof. Andreas Terfort, Goethe-Universität Frankfurt for providing PDMS stamps and finantial support from FWO Odysseus Program under G0D0115N Project.

Appendix A. Supporting information

Supplementary data associated with this article can be found in the online version at doi:10.1016/j.colsurfa.2023.131125.

References

[1] E.T. Castellana, P.S. Kremer, Solid supported lipid bilayers: from biophysical studies to sensor design, Surf. Sci. Rep. 15 (2006) 429–444.
[2] A. Kilic, F.N. Koc, Biomimetic lipid bilayers on solid surfaces: models for biological interactions, Surf. Innov. 4 (2016) 141–157.
[3] T.N. Sut, B.K. Yoon, W.Y. Jeon, J.A. Jackman, N.J. Cho, Supported lipid bilayer coatings: fabrication, bioconjugation, and diagnostic applications, App, Mater. Today 24 (2021), 101183.
[4] J. Kurniawan, J.F. Ventrici de Souza, A.T. Dang, G.Y. Liu, T.L. Kuhl, Preparation and characterization of solid-supported lipid bilayers formed by Langmuir-Blodgett deposition: A tutorial, Langmuir 34 (2018) 15622–15639.
[5] A.C. Simonsen, L.A. Bagatolli, Structured of spin-coated lipid films and domain formation in supported membranes formed by hydration, Langmuir 20 (2004) 9720–9728.
[6] R. Richter, A. Mukhopadhyay, A. Brisson, Pathways of vesicle deposition on solid surfaces: a combined QCM-D and AFM study, Biophys. J. 85 (2003) 3035–3047.
[7] I. Reviakine, A. Brisson, Formation of supported lipid bilayers from unilamellar vesicles investigated by atomic force microscopy, Langmuir 16 (2000) 1806–1815.
[8] R. Tero, Substrate effects on the formation process, structure and physicochemical properties of supported lipid bilayers, Materials 5 (2012) 2658–2680.
[9] T.K. Lind, M. Cárdenas, H.P. Wacklin, Formation of supported lipid bilayers by vesicle fusion: effect of deposition temperature, Langmuir 30 (2014) 7259–7263.
[10] L. Redondo-Morata, P. Losada-Pérez, M.I. Giannotti, Lipid bilayers: phase behavior and nanomechanics, Curr. Top. Membr. 86 (2020) 1–55.
[11] M. Egger, S.P. Heyn, H.E. Gaub, Synthetic lipid-anchored receptors based on the binding site of a monoclonal antibody, Biochim. Biophys. Acta 1104 (1992) 45–54.
[12] D. Meléndrez, T.A. Jowitt, M. Illiut, A.F. Verre, S. Goodwin, A. Vijayaraghavan, Adsorption and binding dynamics of graphene-supported phospholipid membranes using the QCM-D technique, Nanoscale 10 (2017) 2555–2567.
[13] V.I. Silin, H. Wieder, J.T. Woodward, G. Valincius, A. Offenhausser, A.L. Plant, The role of surface free energy on the formation of hybrid bilayer membranes, J. Am. Chem. Soc. 124 (2002) 14676–14683.
[14] E. Kalb, S. Frey, L.K. Tamm, Formation of supported planar bilayers by fusion of vesicles to supported phospholipid membranes, Biochim. Biophys. Acta 1003 (1992) 307–316.
[15] S. Lingler, I. Rubinstein, W. Knoll, A. Offenhauser, Fusion of small unilamellar vesicles to alkanethiol and thiolipid self-assembled monolayers on gold, Langmuir 13 (1997) 7085–7091.
[16] C.W. Meuse, G. Niaura, M.L. Lewis, A.L. Plant, Assessing the molecular structure of alkanethiol monolayers in hybrid lipid bilayer membranes with vibrational spectroscopies, Langmuir 14 (1998) 1604–1611.

[17] L.M. Williams, S.D. Evans, T.M. Flynn, A. Marsh, P.F. Knowles, R.J. Bushby, N. Boden, Kinetics of the unrolling of small unilamellar vesicles onto self-assembled monolayers, Langmuir 13 (1997) 751–757.
[18] G.H. Zan, C. Tan, M. Deserno, F. Lanni, M. Lösche, Hemifusion of giant unilamellar vesicles with planar hydrophobic surfaces: a fluorescence microscopy study, Soft Matter 8 (2012) 10877.
[19] S. Krueger, C.W. Meuse, C.F. Majkrzak, J.A. Dura, N.F. Berk, M. Tarek, A.L. Plant, Investigation of hybrid bilayer membranes with neutron reflectometry: Probing the interactions of melittin, Langmuir 17 (2001) 511–521.
[20] A.L. Plant, M. Brigham-Burke, E.C. Petrella, D.J. O'Shannessy, Phospholipid/alkanethiol bilayers for cell-surface receptor studies by surface plasmon resonance, Anal. Biochem. 226 (1995) 342–348.
[21] G. Puu, I. Gustafson, Planar lipid bilayers on solid supports from liposomes – factors of importance for kinetics and stability, Biochim. Biophys. Acta 1327 (1997) 149–161.
[22] C.A. Keller, B. Kasemo, Surface specific kinetics of lipid vesicle adsorption measured with a quartz crystal microbalance, Biophys. J. 75 (1998) 1397–1402.
[23] Z. Zhi, I.Y. Hasan, A. Mechler, Formation of alkanethiol supported hybrid membranes revisited, Biotechnol. J. 13 (2018) 1800101.
[24] T.N. Sut, S.W. Tan, W.Y. Jeon, B.K. Yoon, N.J. Cho, J.A. Jackman, Streamlined fabrication of hybrid lipid bilayer membranes on titanium oxide surfaces: A comparison of one- and two-tail SAM molecules, Nanomaterials 12 (2022) 1153.
[25] A.L. Plant, Self-assembled phospholipid/alkanethiol biomimetic bilayers on gold, Langmuir 9 (1993) 2764–2767.
[26] Z. Peng, J. Tang, X. Han, E. Wang, S. Dong, Formation of a supported hybrid bilayer membrane on gold: A sterically enhanced hydrophobic effect, Langmuir 18 (2002) 4834–4839.
[27] J.T. Woodward, C.W. Meuse, Mechanism of formation of vesicle fused phospholipid monolayers on alkanethiol self-assembled monolayer supports, J. Colloid Interface Sci. 334 (2009) 139–145.
[28] J.C. Love, L.A. Estroff, J.K. Kriebel, R.G. Nuzzo, G.M. Whitesides, Self-assembled monolayers of thiolates on metals as a form of nanotechnology, Chem. Rev. 105 (2005) 1103–1169.
[29] A.N. Parikh, Membrane-substrate interface: phospholipid bilayers at chemically and topographically structured surfaces, Biointerphases 3 (2008) FA22.
[30] M. Wang, W. Zhan, Mimicking photosynthesis with electrode-supported lipid nanoassemblies, Acc. Chem. Res. 49 (2016) 2551–2559.
[31] C. Li, M. Wang, M. Ferguson, W. Zhan, Phospholipid/aromatic thiol hybrid bilayers, Langmuir 31 (2015) 5228–5234.
[32] S. Yokota, H. Kuramochi, K. Okubo, A. Iwaya, S. Tsuchiya, T. Ichiki, Extracellular vesicles nanoarray technology: Immobilization of individual extracellular vesicles on nanopatterned polyethyleneglycol-lipid conjugate brushes, Plos One 14 (2019), e0224091.
[33] S. Neupane, P. Losada-Pérez, S. Vivegnis, Z. Mekhalif, J. Delhalle, A. Bashir, F. U. Renner, Two-step nanoscale approach for well-defined complex films on Au surfaces, Langmuir 34 (2018) 66–72.
[34] E.L. Florin, M. Rief, H. Lehmann, M. Ludwig, C. Dornmair, V.T. Moy, H.E. Gaub, Sensing specific molecular interactions with the atomic force microscope, Biosens. Bioelectron. 10 (1995) 895–901.
[35] S.J. Atwood, Y. Choi, Z. Leonenko, Preparation of DOPC and DPPC supported planar lipid bilayers for atomic force miscroscopy and atomic force spectroscopy, Int. J. Mol. Sci. 14 (2013) 3514–3539.
[36] R. Lipowsky, U. Seifert, Adhesion of vesicles and membranes, Mol. Cryst. Liq. Cryst. 202 (1991) 17–25.
[37] D.K. Owens, R.C. Wendt, Estimation of the surface free energy of polymers, J. Appl. Polym. Sci. 13 (1969) 1741–1747.
[38] T. Heimburg, Thermal biophysics of membranes, Wiley-VCH Verlag (2007).
[39] E.G. Kelley, P.D. Butler, M. Nagao, Scaling of membrane ridigity with domain area fraction, Soft Matter 15 (2019) 2762–2767.
[40] T.N. Murugova, P. Balgavy, Molecular volumes of DOPC and DOPS in mixed bilayers of multilamellar vesicles, Phys. Chem. Chem. Phys. 16 (2014) 18211.
[41] M.L. Schmidt, L. Ziani, M. Boudreau, J.H. Davis, Phase equilibria in DOPC/DPPC: conversion from gel to subgel in two component mixtures, J. Chem. Phys. 131 (2009), 175103.
[42] R.N.A.H. Lewis, N. Mak, R.N. McElhaney, A differential scanning calorimetry study of the thermotropic phase behavior of model membranes composed of phosphatidylcholines containing saturated fatty acyl chains, Biochemistry 26 (1987) 6118–6126.
[43] N. Bibissidis, K. Betlem, G. Cordoyiannis, F. Prista-von Bonhorst, J. Goole, J. Raval, M. Daniel, W. Gozdz, A. Iglic, P. Losada-Pérez, Correlation between adhesion strength and phase behavior in solid-supported lipid membranes, J. Mol. Liq. 320 (2020), 114492.
[44] T.H. Fang, W.Y. Chang, C.I. Weng, C.N. Fang, Surface and mechanical characteristics of alkanethiol self-assembled monolayers, J. Adv. Microsc. Res 6 (2011) 24–28.
[45] L. Bar, F. Perissinotto, L. Redondo-Morata, M.I. Giannotti, J. Goole, P. Losada-Pérez, Interactions of hydrophilic quantum dots with defect-free and defect containing supported lipid bilayers, Coll. Surf. B Biointerfaces 210 (2022), 112239.
[46] K.L. Weirich, J.N. Israelachvili, D.K. Fygenson, Bilayer edges catalyze supported lipid bilayer formation, Biophys. J. 98 (2010) 85–92.
[47] T.K. Lind, M. Cárdenas, Understading the formation of supported lipid bilayers via vesicle fusion−A case that exemplifies the need for the complementary method approach, Biointerphases 11 (2016), 020801.
[48] W. Helfrich, M.M. Kozlov, Flexibility and roughness of mixed and partially polymerized bilayers in terms of the had model and local bending frustration, J. Phys. Fr. II 4 (1994) 1427–1438.
[49] S.K. Pramanik, S. Seneca, A. Ethirajan, S. Neupane, F.U. Renner, P. Losada-Pérez, Ionic strength dependent vesicle adsorption and phase behavior of anionic phospholipids on a gold substrate, Biointerphases 11 (2016), 019006.
[50] S. Neupane, Y. De Smet, F.U. Renner, P. Losada-Pérez, Quartz crystal microbalance with dissipation monitoring: A versatile tool to monitor phase transitions in biomimetic membranes, Front. Mater. 5 (2018) 46.
[51] O. Saavedra, T.F.D. Fernandes, P.E. Milhiet, L. Costa, Compression, rupture, and puncture of model membranes at the molecular scale, Langmuir 36 (2020) 5709–5716.
[52] K. El Kirat, S. Morandat, Y.F. Dufrêne, Nanoscale analysis of supported lipid bilayers using atomic force microscopy, Biochim. Biophys. Acta 2010 (1798) 750–765.
[53] Y. Duan, Y. Liu, J. Li, H. Wang, S. Wen, Investigation on the nanomechanics of liposome adsorption on titanium alloys: Temperature and Loading effects, Polymers 10 (2018) 383.
[54] J.D. Unsay, K. Cosentino, A.J. García-Sáez, Atomic force microscopy imaging and force spectroscopy of supported lipid bilayers, J. Vis. Exp. 101 (2015) 52867.
[55] A.T.A. Jenkins, R.J. Bushby, S.D. Evans, W. Knoll, A. Offenhäusser, S.D. Ogier, Lipid vesicle fusion on μCP patterned self-assembled monolayers: effect of pattern geometry on bilayer formation, Langmuir 18 (2002) 3176–3180.
[56] S. Neupane, N.A. Rivas, P. Losada-Pérez, J. D'Haen, H. Noei, T.F. Keller, A. Stierle, M. Rudolph, A. Terfort, O. Bertran, D. Crespo, A. Kokalj, F.U. Renner, A model study on controlling dealloying corrosion attack by lateral modification of surfactant inhibitors, NPJ Mater. Degrad. 5 (2021) 1–6.
[57] A. Valencia Ramirez, G. Bonneaux, A. Terfort, P. Losada-Pérez, F.U. Renner, Nanomechanical stability of laterally heterogeneous films of corrosion inhibitors obtained by microcontact printing on model Au surfaces, Langmuir 38 (2022) 15614–15621.